Arabian Journal of Geosciences (2019) 12: 46
https://doi.org/10.1007/s12517-018-4184-0

S. I. BIOCHAR

Application of the biochar derived from orange peel for effective biosorption of copper and cadmium in batch studies: isotherm models and kinetic studies

M. T. Amin [1,2] · A. A. Alazba [1,3] · M. Shafiq [1]

Received: 4 September 2018 / Accepted: 21 December 2018 / Published online: 10 January 2019

Abstract
Orange peel biochar (OP_b) was used as an adsorbent to investigate its potential in the removal of copper (Cu^{2+}) and cadmium (Cd^{2+}). The adsorption data were modeled using different isotherm models and reaction kinetics after optimizing reaction parameters such as solution pH, equilibrium contact time, OP_b dose, and initial metal concentrations. Scanning electron microscopy images showed porous and irregular surfaces in OP_b prior to the sorption process. Energy dispersive X-ray results depicted successful adsorption of the metal ions. An equilibrium time of 30 min was estimated for low initial metal ion concentrations (25–50 mg L^{-1}). Metal adsorption and removal efficiency increased with an increase in the initial solution pH from 2.5 to 5.5. The adsorption capacity increased as the initial metal concentration varied from 25 to 200 mg L^{-1}; the removal efficiency decreased from 99% to about 41% and 52% for Cu^{2+} and Cd^{2+}, respectively. A decrease in adsorption capacity with an increase in metal removal efficiency was observed by increasing the OP_b dose from 0.2 to 1.4 g. Langmuir and Temkin isotherm models best fit the adsorption data for Cu^{2+} and Cd^{2+}, with a coefficient of determination (R^2) value of 0.85. Other isotherm models fit the adsorption data in the following order: Temkin > D-R > Halsey and Freundlich > H-J and Halsey > D-R > Langmuir > Freundlich > H-J, respectively. The chemisorptive nature of OP_b for the adsorption of both ions was suggested based on R^2 values close to unity (1.0) in a pseudo-second-order kinetic model.

Keywords Adsorption capacity · Batch parameters · Biochar · Heavy metal ions · Langmuir and Freundlich · Pseudo-second-order · Removal efficiency

Introduction

The presence of heavy metals in drinking water is a serious threat to human health and the ecosystem. Rapid industrialization and urbanization have resulted in elevated levels of various heavy metals in water bodies. These metals and their compounds are highly carcinogenic due to their non-degradability and long-term persistence in nature. Continuous exposure to them leads to severe disorders in animals and humans such as cardiovascular diseases, cancer, and neurological, respiratory, liver, and kidney failure (Bilal et al. 2013; Purkayastha et al. 2014; Shafiq et al. 2018). Copper (Cu^{2+}) and cadmium (Cd^{2+}), which are among the most commonly occurring heavy metals, are of critical importance because of their use in a range of industries such as paints, batteries, coatings, solar cells, different alloys, building construction, and electrical and electronic items for the preparation of different useful end products. Untreated effluent released into the environment from these industries possesses higher amounts of Cu^{2+} and Cd^{2+} that pollute the natural ecosystem. These metals can affect the ecosystem even after several years of their introduction into the environment (Ahmad et al. 2018). Therefore, the high levels of these metals in water reservoirs are a threat to living organisms in the oceans, and to animals, plants, and human health. Therefore, it is crucial to

This article is part of the Topical Collection on *Implications of Biochar Application to Soil Environment under Arid Conditions*

✉ M. T. Amin
mtamin@ksu.edu.sa

[1] Alamoudi Water Research Chair, King Saud University, Riyadh, Saudi Arabia

[2] Department of Environmental Sciences, COMSATS Institute of Information Technology, Abbottabad 22060, Pakistan

[3] Agricultural Engineering Department, King Saud University, Riyadh, Saudi Arabia

develop cost-effective, eco-friendly, and sustainable remediation technologies to remove these metals from wastewater as well as to treat metal-contaminated wastewater before discharging it into natural water bodies (Barakat 2011).

So, far numerous technologies, like ion exchange, electrocoagulation membrane filtration, and desalination, have been used to remove heavy metals from inorganic effluents (Mohsen et al. 2003; Kumar et al. 2004, 2010; Alkhashman 2005; Mavrov et al. 2006; Lin et al. 2009; Kim and Choi 2010; Danilchenko et al. 2011; Dermentzis et al. 2011). However, these techniques are considered inefficient to counter heavy metal contamination mainly because of their high cost, high energy requirements and reagent consumption, and generation of toxic sludge in addition to the incomplete removal of heavy metal ions (Krishnani et al. 2008). Among various remediation technologies, adsorption is the most commonly used and a widely accepted technique. The adsorption technology, using different adsorbents, has been proved as a very promising technique for removing heavy metals and offers significant advantages over the conventional treatment processes due to lower costs, profitability, availability of raw materials, ease of operation, high efficiency, and suitability to a wide variety of industrial metal-containing effluents (Volesky and Holan 1995). Adsorbents such as plant materials and activated carbon are being used for the adsorption of heavy metals (Han et al. 2006; Srivastava et al. 2008; Tan and Xiao 2009; Ebrahimi et al. 2013; Akar et al. 2013; Amin et al. 2017a).

Biochar-based materials have recently been introduced as low-cost, eco-friendly, and efficient green-sorbents for heavy metal removal (Ahmad et al. 2017). Biochar is a black, solid, and stable porous carbonaceous material possessing a large surface area and functional groups and is produced by pyrolysis of different types of waste biomass (Ahmad et al. 2017). Biochar has been successfully used for heavy metal removal because of its distributed pore size, high surface area, higher adsorption capacities, ease of preparation, and presence of several functional groups (Ahmad et al. 2014). Researchers have suggested an optimum temperature higher than 500 °C for biochar production from agricultural wastes due to a high surface area and porosity in addition to the stable carbon contents (Karim et al. 2015; Tag et al. 2016).

Reusing and recycling the agricultural and food wastes and converting into biochar can provide low-cost and efficient sorbents for the remediation of a range of environmental contaminants. For instance, biochar produced from agriculture and food wastes such as banana peels, rice straw, corn straw, rice husk, and dairy manure are considered as low-cost sorbents and have exhibited excellent results in heavy metal removal from wastewaters (Cao et al. 2009; Tong et al. 2011; Xu et al. 2013; Chi et al. 2017; Amin et al. 2017b). Likewise, orange peel is also an agricultural as well as a food waste which is abundant in various parts of the world, as 75% of total citrus production consists of oranges (Rafiq et al. 2016). Orange peel mainly contains cellulose, hemicellulose, and pectin in higher proportions (Chen and Chen 2009) Therefore, it was hypothesized that pyrolyzing the orange peel waste biomass may produce efficient and low-cost biochar with a higher sorption capacity which can subsequently be applied for Cu^{2+} and Cd^{2+} removal from aqueous solutions. Thus, the purpose of this study was to explore the potential applicability of preparing biochar of an agro-industrial waste obtained from orange peels and using it as a bio-sorbent material for Cu^{2+} and Cd^{2+} removal from aqueous solutions in batch experiments.

Materials and methods

The peel of orange fruit (*Citrus reticulata*) was used as the original material for the preparation of biochar. The fruit peels of oranges were collected from a local plant in Riyadh, Saudi Arabia, and the pyrolyzed product of the orange peels, i.e., its biochar (OP_b), was prepared at 800 °C by the method used for preparing banana biochar, as described in a previous study (Amin et al. 2017b).

All chemicals used were of analytical reagent grade and appropriate amounts of copper sulfate pentahydrate ($CuSO_4 \cdot 5H_2O$; AR grade Merck, Germany) and cadmiumnitrat-4-hydrate ($Cd(NO_3)_2 \cdot 4H_2O$; AR grade Merck, Germany) were added in distilled-deionized water for preparing stock solutions of Cu^{2+} and Cd^{2+}, respectively. Preservation of the stock solution and its dilutions to prepare metal solutions with different initial concentrations and pH adjustment was in accordance with a previously published report (Amin et al. 2017a).

The metal sorption performance of OP_b for Cu^{2+} and Cd^{2+} in batch mode was performed by suspending the appropriate amount of OP_b in 100 mL of metal solutions with the required initial concentrations. Suspensions were kept under constant agitation (220 rpm) and temperature (30 °C) for a specified contact time. The supernatant solutions after centrifuge and filtration were analyzed using flame atomic absorption spectrometry (FAAS, Thermo Scientific, ICE 3000 Series, Cambridge, UK) and the quantity of Cu^{2+} and Cd^{2+} adsorbed onto OP_b at equilibrium and the removal efficiency (R, %) was evaluated using the equations given below:

$$q_e = (C_0 - C_e)\,\frac{V}{M} \tag{1}$$

$$R = \left[\frac{(C_0 - C_e)}{C_o}\right] 100 \tag{2}$$

where q_e is the adsorbed equilibrium concentrations of Cu^{2+} or Cd^{2+} on to OP_b (mg g^{-1}), V and M are the volume of the solution (L) and mass of OP_b (g), respectively, while C_e and C_o represent the equilibrium and initial metal concentrations (mg L^{-1}), respectively.

Results and discussion

Characteristics of adsorbent material

Scanning electron microscopy (SEM, TESCAN VEGA 3 SBU USA) images of the OP_b before and after Cu^{2+} and Cd^{2+} sorption are shown in Fig. 1.

The OP_b prior to the sorption process showed porous and irregular surfaces (Fig. 1a) which helped the biochar to sorb metal ions onto the surfaces, as shown in Fig. 1b and c (Mary et al. 2016). The white particles on the biochar surfaces might be due to the sorption of Cu^{2+} and Cd^{2+} ions on the surfaces and pores (Fig. 1b and c, respectively). Hence, the presence of Cu^{2+} and Cd^{2+} on the surface of biochar materials suggested the occurrence of some physiochemical interactions between the functional groups present on the surface of the adsorbent and the metals ions (Suliman et al. 2016). These results were further supported by performing an energy dispersive X-ray (EDX) analysis (Fig. 2).

On a percent weight basis, the main components of OP_b before the sorption process, as indicated in Fig. 2a, included carbon (C, 36.37%), oxygen (O, 46.99%), magnesium (Mg, 1.29%), silicon (Si, 0.61%), potassium (K, 9.54%), and calcium (Ca, 5.20%) (Budai et al. 2014). The changes in the proportions of these components in post-sorption samples are shown in Fig. 2b and c. The O/C molar ratios were calculated by using the C and O percent weight, which is used to determine the degree of aromaticity and carbonization degree of biochar (Ma et al. 2016). Hence, these EDX results confirmed that Cu^{2+} and Cd^{2+} ions were adsorbed successfully on the surface of OP_b due to strong physiochemical interactions (Kim et al. 2012).

The Fourier–transform infrared spectroscopy (FTIR) using a ZnSe-attenuated total reflection (ATR) crystal with a Bruker Alpha-E spectrometer was used to find the active functional groups on the surface of the biochar responsible for metal ion adsorption. The analyses of these spectra were based on previously published data (Kloss et al. 2012; Claoston et al. 2014).

Abrupt changes in the FTIR spectra were observed as the OP_b was charred at 800 °C (Fig. 3). It has been reported previously that the number of bands representing the functional groups disappeared as the charring temperature increased to 700 °C or above (Yuan et al. 2011; Jindo et al. 2014; Usman et al. 2016). The most prominent peak in orange peel biomass was seen at 1017.72 cm^{-1}, which represented SiO_2 and was lost in OP_b (Jindo et al. 2014). Likewise, a band describing C–O also disappeared during the pyrolysis process (Jindo et al. 2014; Jouiad et al. 2015). New stretching bands appeared at 1417.46 and 858.64 cm^{-1} in OP_b after sorption of Cu^{2+} and Cd^{2+} ions, respectively. The new bands in the OP_b sample after Cd^{2+} adsorption were ascribed as C=C and C–H aromatic groups. These were more intense as compared to the OP_b after the Cu^{2+} adsorption, suggesting that the interactions between Cd^{2+} ions and the OP_b surface were stronger than the interactions between Cu^{2+} ions and the OP_b surface (Lammers et al. 2009; Inyang et al. 2012, 2016).

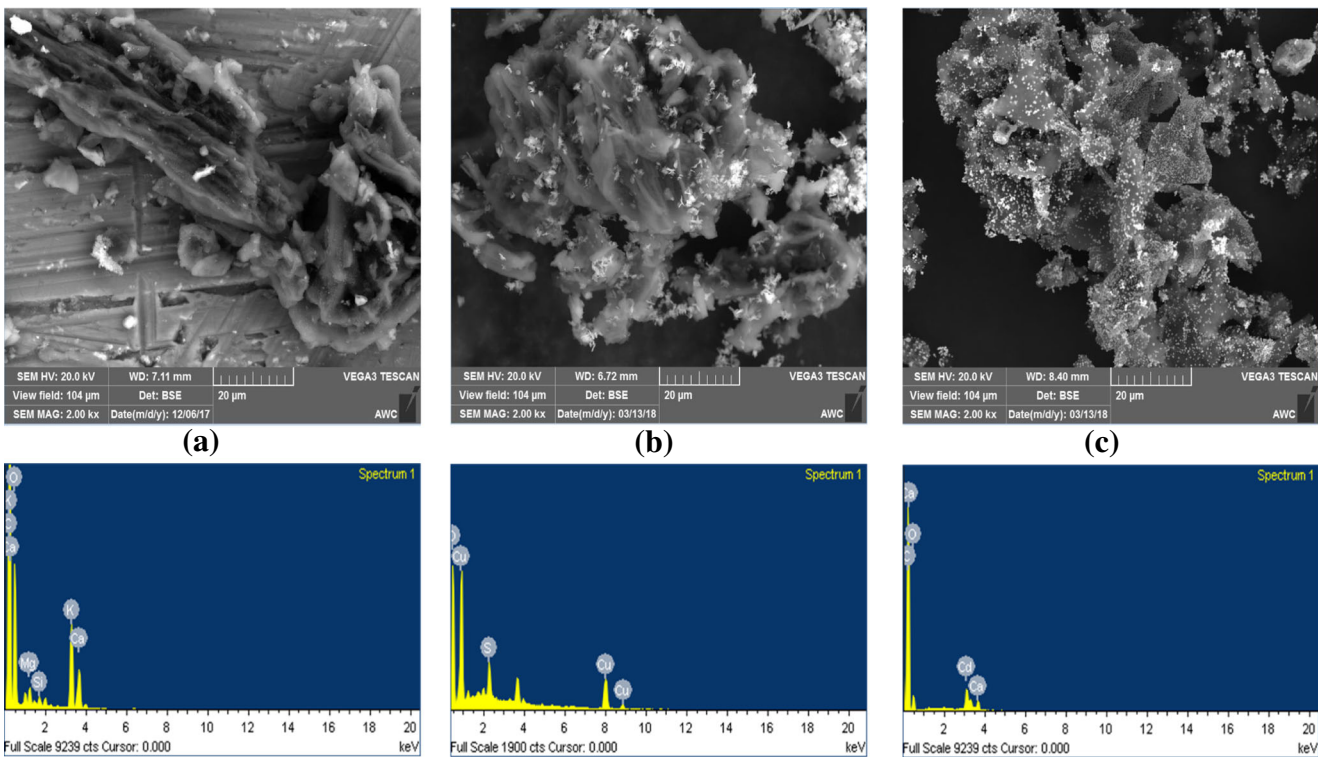

Fig. 1 SEM and EDX spectra of OP_b before (**a**) and after Cu^{2+} (**b**) and Cd^{2+} (**c**) adsorption

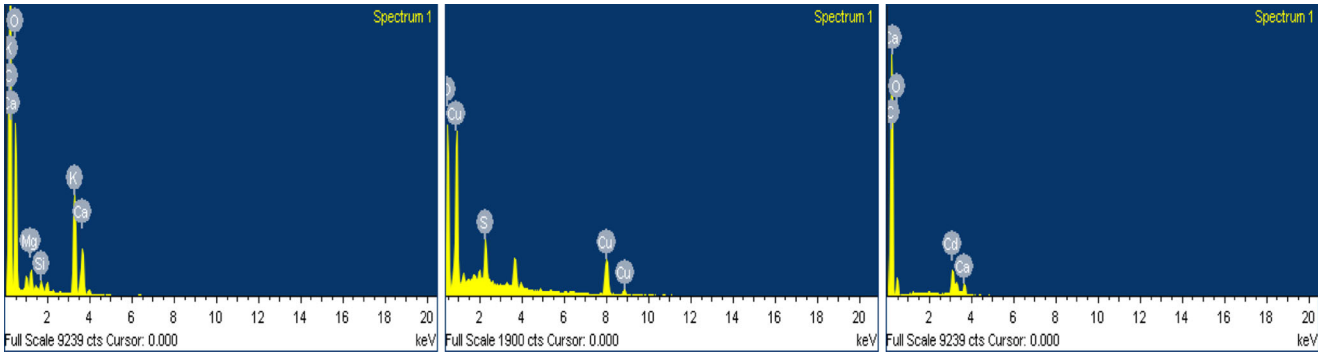

(a)

Element	Weight %	Atomic %
C	36.37	47.22
O	46.99	45.79
Mg	1.29	0.83
Si	0.61	0.34
K	9.54	3.81
Ca	5.2	2.02
Totals	100	

(b)

Element	Weight %	Atomic %
C	67.52	78.69
O	21.26	18.6
S	1.09	0.48
Cu	10.13	2.23
Totals	100	

(c)

Element	Weight %	Atomic %
C	65.11	79.93
O	18.8	17.33
Ca	2.67	0.98
Cd	13.42	1.76
Totals	100	

Fig. 2 EDX spectra and elemental weight % tables of OP_b before (**a**) and after Cu^{2+} (**b**) and Cd^{2+} (**c**) adsorption

Effects of solution pH, contact time, initial metal concentrations, and adsorbent dose

The adsorption experiments were performed in triplicate for statistical analysis and to eliminate any experimental error. The required amount of OP_b was suspended in 50 or 100 mL conical flasks containing metal solutions of Cu^{2+} or Cd^{2+} for obtaining the required dose of the adsorbent.

Influence of contact time

Time-series experiments were performed to find the effects of contact time on the removal of the heavy metal ions by OP_b, as shown in Fig. 4a and b. Solution pH was kept constant at 5 ± 0.5 with the OP_b dose at 1.0 g. Initial metal ion concentrations were maintained in the range 25–100 mg L^{-1} while samples were subject to 6 h of contact time.

A rapid adsorption was observed for both the heavy metal ions during the first 15–30 min. Thereafter, a slower rate of adsorption was observed mainly due to a decreased or lesser number of active sites. The maximum removal efficiency (about 99%) of both Cu^{2+} and Cd^{2+} was attained after a contact time of about half an hour at low initial metal concentrations (25–50 mg L^{-1}), as shown in Fig. 4a and b, respectively. For high initial metal concentrations (75–100 mg L^{-1}), an extended equilibrium time of about 3 h was observed, following a very slow metal uptake. An identical behavior of metal removal was seen for both the heavy metal ions with a slightly higher removal of Cu^{2+} than Cd^{2+}.

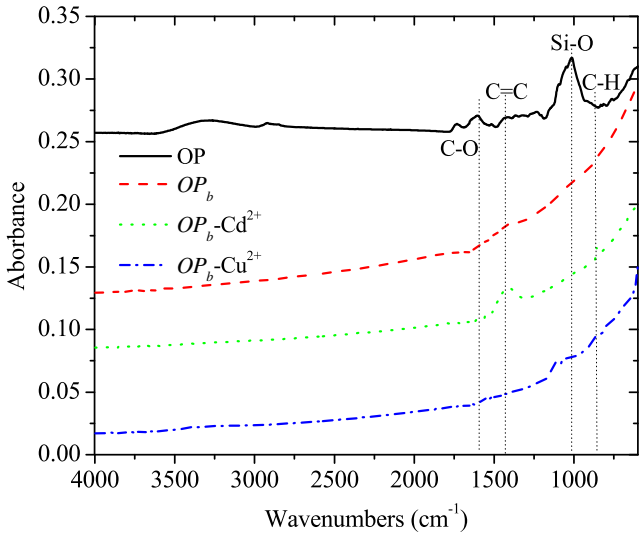

Fig. 3 FTIR spectra of orange peels waste biomass and OP_b with and without adsorption of Cu^{2+} and Cd^{2+}

Influence of solution pH

Adsorption process is greatly influenced by controlling the pH of the aqueous solution (Areco and Afonso 2010). Batch tests were performed in the pH range of 2.5–5.5 in order to recognize the influence of pH, as shown in Fig. 5. A 1.0 g of OP_b was stirred for a contact time of 30 min using 50 and 75 mg L^{-1} of Cd^{2+} and Cu^{2+}, respectively.

The initial solution pH is critical for metal biosorption (O'Connell et al. 2008; Al-Ghouti et al. 2010), which is also evident from results of the current study where the maximum metal uptake was seen at a pH value of 5.0. The metal removal efficiency increased from 62 to 84% and from 61 to 96% for Cu^{2+} and Cd^{2+}, respectively, as the initial solution pH increased from 3.5 to 5.5 (Fig. 5). A very low adsorption capacity in a strong acidic environment (pH 2.5) could be ascribed to the

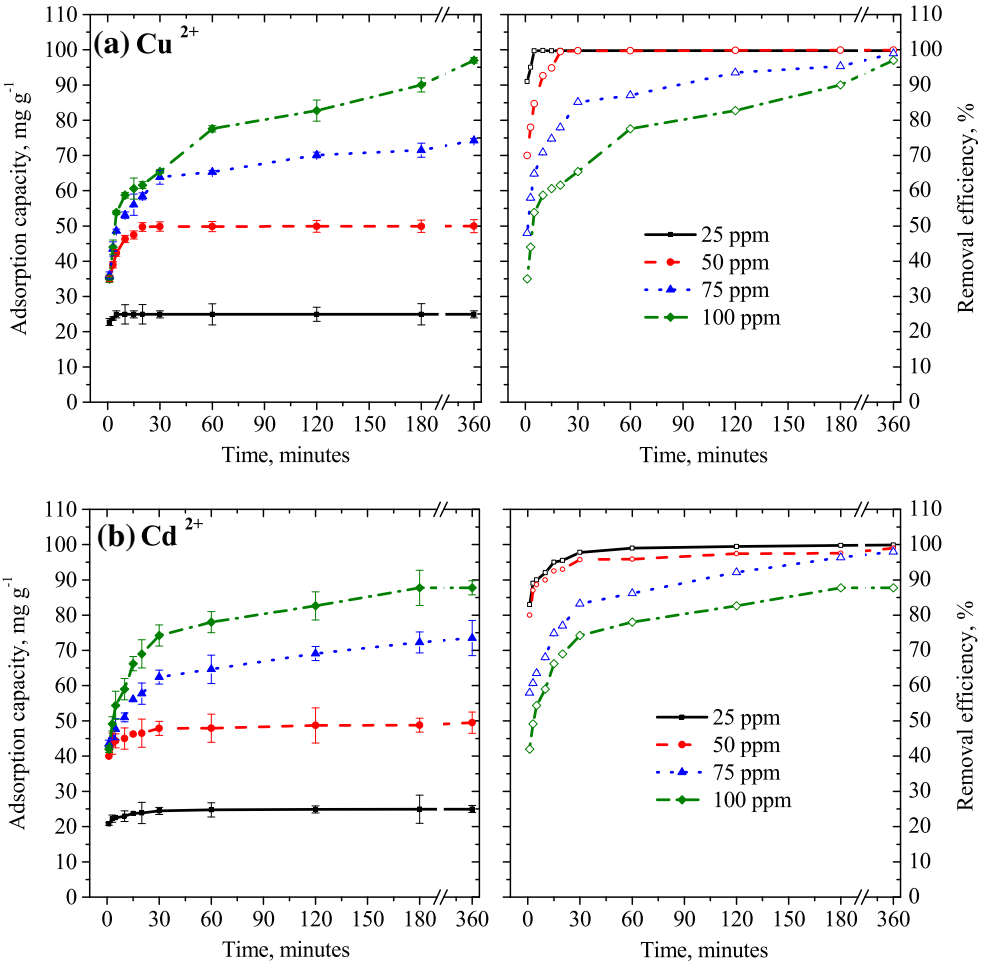

Fig. 4 Changes in removal efficiency and adsorption capacity of Cu^{2+} (**a**) and Cd^{2+} (**b**) with contact time

competition between the divalent metal ions on the sorption sites of OP_b and excess hydrogen (Al-Ghouti et al. 2003). At high pH (5.0 and above) values, the decreased positive surface charge density along with the availability of more negative charges results in a higher removal efficiency (Chen and Lin 2001). The precipitation of hydroxides of the metals at high pH (6.0 and above) (Snoeyink and Jenkins 1980) makes true biosorption impossible, thus suggesting that the pH value of 5.5 was suitable for the adsorption experiments in this study.

Influence of initial metal concentrations

The adsorption experiments with varying initial metal concentrations (25–200 mg L^{-1}) were performed using fixed values of OP_b

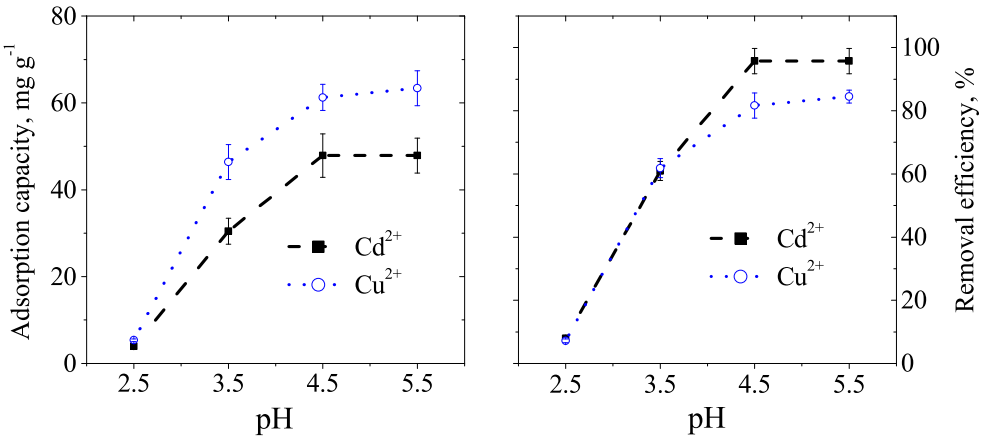

Fig. 5 Changes in adsorption capacity and removal efficiency of Cu^{2+} and Cd^{2+} with solution pH

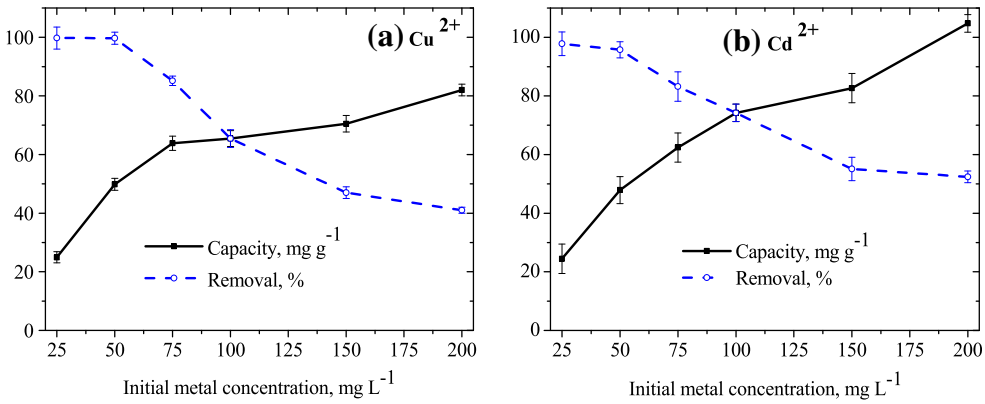

Fig. 6 Changes in metal adsorption capacity of both heavy metal ions with initial metal concentration

(1.0 g), equilibrium contact time (30 min), and solution pH (5.5 ± 0.5). Changes in adsorption capacity of OP_b and removal efficiency of Cu^{2+} and Cd^{2+} are presented in Fig. 6a and b, respectively.

As expected, higher initial concentrations increased the sorption rate and the adsorption capacity increased sharply in the beginning (up to about 75–100 mg L^{-1}). However, a slower uptake was seen further up to 200 mg L^{-1}. The optimum adsorption capacity for Cu^{2+} and Cd^{2+} was estimated as 82 and 105 mg g^{-1}, respectively, when using the highest initial metal concentration (200 mg L^{-1}), probably due to the higher interaction between metal ions and OP_b (Das and Guha 2007; Rathinam et al. 2010). Percent removal, however, was highest (99%) at the lowest used initial metal concentrations (25 mg L^{-1}) but decreased almost linearly by increasing the initial metal concentrations and reached about 41 and 52% for Cu^{2+} and Cd^{2+}, respectively, at the highest used initial metal concentration (200 mg L^{-1}). This could be attributed to rapid saturation of active sorption sites on the surface of OP_b at high initial metal concentrations (Malkoc et al. 2006; Bhaumik et al. 2013; Al-Homaidan et al. 2014; Putra et al. 2014).

Influence of adsorbent dose

The effect of different OP_b doses (0.2 to 1.4 g) was studied at a fixed contact time (30 min), pH (5 ± 0.5), and Cu^{2+} and Cd^{2+} concentrations of 75 and 50 mg L^{-1}, respectively (Fig. 7).

Results presented in Fig. 7 suggest a decrease in the adsorption capacity while the removal efficiency of both heavy metal ions increased almost linearly by increasing the OP_b concentration. For Cd^{2+}, however, 1.0 g of OP_b can be considered optimum for maximum adsorption capacity or removal efficiency (Fig. 7) due to the unsaturation of adsorption sites (Huang et al. 2011) by increasing the adsorbent dose at fixed concentrations, i.e., 50 mg L^{-1}. The results could be attributed to the increased number of adsorbent particles, active sites or functional groups surrounding the metal cations, and greater availability of surface resulting in stronger metal cation-biochar interactions (Ofomaja and Ho 2007; Uzunoğlu et al. 2014).

Adsorption kinetics and isotherm models

Adsorption kinetics

Adsorption kinetics of both heavy metal ions on to OP_b at various initial concentrations of Cu^2 and Cd^{2+} (25–100 mg L^{-1}) were modeled using pseudo-first-order (Eq. (3)) and pseudo-second-order (Eq. (4)) kinetic models, which comprise of the entire adsorption process including the external film and internal particle diffusion (Özacar and Şengil 2003; Liu and Ren 2006; Crini et al. 2007; Greluk and Hubicki 2010). A time range between 1 min and 6 h was selected at fixed pH (5 ± 0.5) and 1.0 g of OP_b dose.

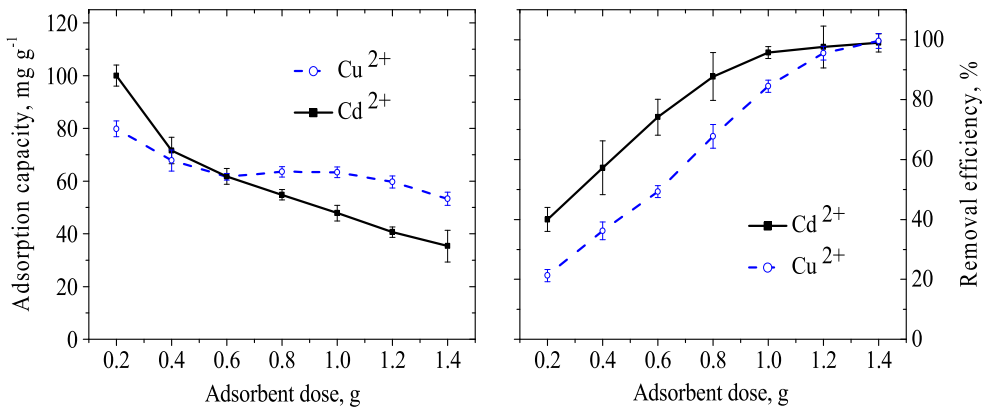

Fig. 7 Changes in removal efficiency and adsorption capacity of Cu^{2+} and Cd^{2+} with adsorbent dose

$$\log(q_e - q_t) = \log q_e - \frac{k_1}{2.303} t \quad (3)$$

$$\frac{t}{q_t} = \frac{1}{k_2 q_e^2} + \frac{1}{q_e} t \quad (4)$$

$$h = k_2 q_e{}^2 \quad (5)$$

where q_t is the amount of metal adsorbed at time t (mg g^{-1}), and k_1 (hr^{-1}) and k_2 (g mg^{-1} min^{-1}) are rate constants of the pseudo-first-order and second-order kinetic models, respectively. These were calculated using the slope and intercept values of the plot of log (q_e-q_t) vs. t and t/q_t vs. t, respectively. As shown in Fig. 8, a relatively poor correlation (based on R^2 values) to the experimental data of both heavy metal ions was observed, corresponding to maximum used initial Cu^{2+} and Cd^{2+} concentrations (100 mg L^{-1}), with the pseudo-first-order kinetic model as compared to the pseudo-second-order kinetic model.

On the other hand, high R^2 values were seen for both heavy metal ions at all the initial concentrations using the pseudo-second-order model, as shown in Table 1. Table 1 also presents the values of k_2, estimated adsorption capacity, and the corresponding initial adsorption rate, h (mg g^{-1} min^{-1}, Eq. (5)), calculated in the pseudo-second-order kinetic model at the respective initial concentrations of Cu^{2+} and Cd^{2+}.

The estimated q_e values showed dissimilarities in the pseudo-first-order model (results not shown). However, $q_{e\ cal}$ was similar to the experimental adsorption capacities ($q_{e\ exp}$) at the respective initial concentrations of Cu^{2+} and Cd^{2+}, as shown in Table 1. Thus, the pseudo-second-order model is more likely to describe the kinetic behavior, indicating that chemisorption can be considered as the rate-controlling factor for the adsorption of the heavy metal ions on to OP_b.

Equilibrium isotherm models

Equilibrium studies were further explained using adsorption isotherms which are used to correlate the residual adsorbate concentration at fixed temperature with that of the equilibrium adsorption capacity (Kiran et al. 2006; Yavuz et al. 2008; Guendy 2010). In this study, two-parameter equilibrium isotherms have been described using Langmuir, Freundlich, Temkin, Halsey, Dubinin–Radushkevich (D-R), and Harkin–Jura (H-J) isotherms. The analysis was performed using a solution temperature of 30 °C at fixed pH (5.5 ± 0.5), equilibrium contact time (30 min), metal ion concentration (200 mg L^{-1}), and OP_b dose (1.0 g).

The Langmuir isotherm model predicts the monolayer coverage of the adsorbate at a specific homogenous site within the adsorbent (Langmuir 1918) and can be expressed using Eq. (6) in its linearized form. The Freundlich isotherm model, on the other hand, assumes a multilayer adsorption (Eq. (7)).

$$\frac{1}{q_e} = \left(\frac{1}{q_{\max} K_L}\right)\frac{1}{C_e} + \frac{1}{q_{\max}} \quad (6)$$

$$\log q_e = \log K_F + \frac{1}{n}\log C_e \quad (7)$$

where q_e and C_e are already defined above, q_{max} is the monolayer capacity of OP_b in the Langmuir model (mg g^{-1}), K_L is the Langmuir adsorption constant (L mg^{-1}), $1/n$ is the heterogeneity factor that determines the intensity and feasibility of the adsorption process in the Freundlich model, and K_F is the Freundlich constant (L g^{-1}). The linearized plots of $1/q_e$ vs. $1/C_e$ (Fig. 9a) and log q_e vs. log C_e (Fig. 9b) were used to describe the fit of the equilibrium data in the Langmuir and Freundlich isotherms, respectively. The values of $q_{\max}$ and K_L in the Langmuir isotherm and $1/n$ and K_F in the Langmuir model, as calculated from the linearized plots, are presented in Table 2.

The coefficient of determination (R^2) for the fit of Cu^{2+} and Cd^{2+} adsorption data was calculated as 0.95 and 0.98, respectively (Table 2), reflecting the suitability of the Langmuir isotherm model to describe the adsorption of the heavy metal ions on to OP_b. Additionally, higher values of R^2 for both Cu^{2+} and Cd^{2+} in the Langmuir isotherm as compared to the Freundlich isotherm (0.79 and 0.95 for Cu^{2+} and Cd^{2+}, respectively, Fig. 9b) indicate suitability of the Langmuir model to the adsorption data.

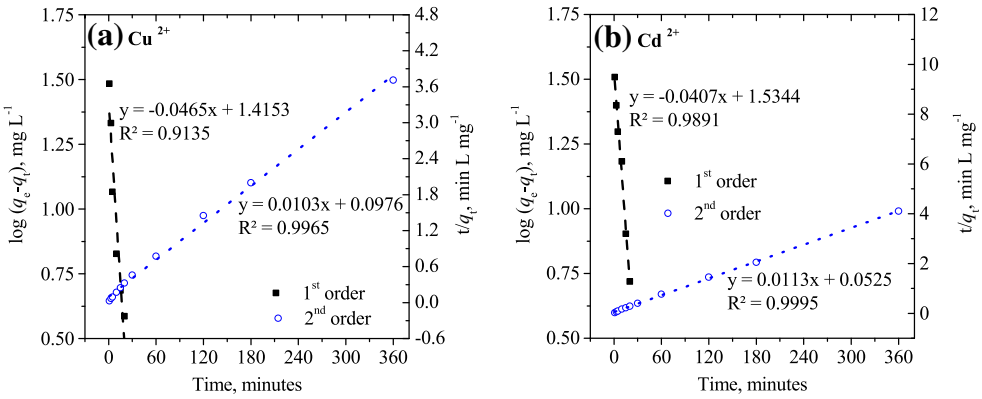

Fig. 8 Kinetic plots of both kinetic models with 250 mg L^{-1} of Cu^{2+} (**a**) and Cd^{2+} (**b**)

Table 1 Parameters of kinetic models for adsorption of Cu^{2+} and Cd^{2+} on to OP_b at 30 °C and pH 5.5 ± 0.5

	$q_{e\ exp}$ (mg g^{-1})	$q_{e\ cal}$ (mg g^{-1})	k_2 (g mg^{-1} min^{-1})	h (mg g^{-1} min^{-1})	R^2
Initial Cu^{2+} conc. (mg L^{-1})					
25	24.938	24.938	0.9459	588.23563	1
50	49.847	50	0.0381	95.2386	1
75	63.864	74.627	0.0029	16.266	0.9995
	100	65.462	97.087	0.0011	10.246
	0.-99-65				
Initial Cd^{2+} conc. (mg L^{-1})					
25	24.452	25	0.063	39.526	1
50	47.875	49.505	0.0185	45.45	0.9999
75	62.414	74.0745	0.003	16.287	0.9995
	100	74.237	88.496	0.0024	19.048
	0.-99-95				

Furthermore, it was hypothesized that OP_b reached its saturation capacity at low initial metal concentration in the Langmuir isotherm. This was evident from lower values of the predicted maximum adsorption capacity (q_{max} as 73 and 81 mg g^{-1}, Table 2) for Cu^{2+} and Cd^{2+}, respectively, as compared to the experimentally attained values ($q_{e\ exp}$ in Table 2) of 82 and 105 mg g^{-1} for Cu^{2+} and Cd^{2+}, respectively. Favorable adsorption was also expected in the Freundlich isotherm as the values of n were situated between 2.0 and 10 (Table 2) for both heavy metal ions, which indicated favorable physical adsorption ($n > 1$) (Tunali et al. 2006).

To take into account the interaction of adsorbent-adsorbate, the Temkin isotherm model (Temkin and Pyzhev 1940), as expressed linearly in Eq. (8), was applied to the adsorption data. In order to confirm the heterogeneous nature of the adsorbent and its suitability for multilayer adsorption, the Halsey isotherm model (Eq. (9)) was used.

$$q_e = \frac{RT}{b_T} \ln C_e + \frac{RT}{b_T} \ln A_T \tag{8}$$

$$\ln q_{e=} \frac{1}{n_H} \ln K_H - \frac{1}{n_H} \ln C_e \tag{9}$$

where A_T and b_T are Temkin constants related to the maximum binding energy and the heat of adsorption (kJ mol^{-1}), respectively, calculated from the linearized plot of q_e vs. ln C_e (Table 2). T and R are the absolute temperature (K) and universal gas constant (8.314 J $mol^{-1}{\cdot}K^{-1}$), respectively. Halsey s isotherm constants, k_H and n_H in Eq. (9) were evaluated using the linearized plot of ln q_e vs. ln C_e (Table 2).

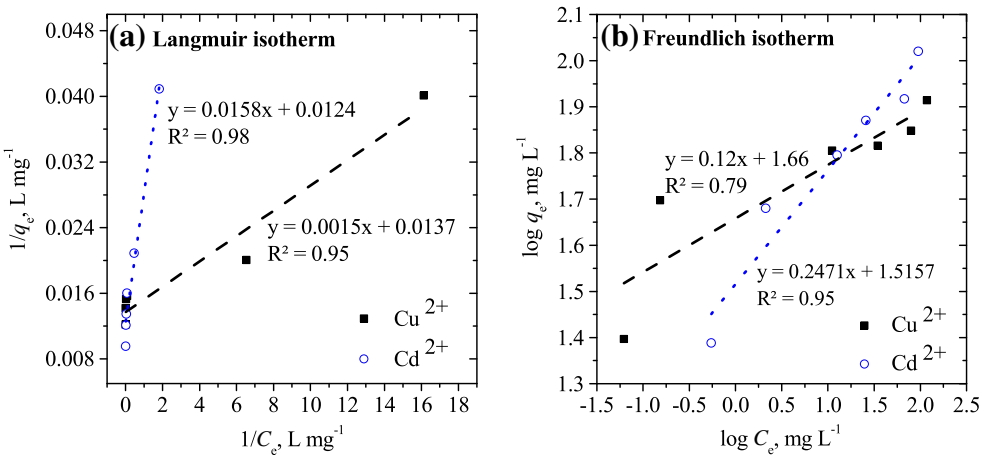

Fig. 9 Linearized Langmuir and Freundlich plots for the adsorption of Cu^{2+} and Cd^{2+} onto OP_b

Table 2 Values of parameters in two-parameter equilibrium isotherm models

Isotherm	Parameter	Cu^{2+}	Cd^{2+}
	$q_{e\ exp}$, mg g^{-1}	82.00	104.76
Langmuir	q_{max}, mg g^{-1}	72.99	80.65
	K_L, L mg^{-1}	9.13	0.78
	R^2	0.95	0.91
Freundlich	K_F, L g^{-1}	47.06	33.98
	q_m, mg g^{-1}	87.19	125.84
	n	8.59	4.05
	R^2	0.80	0.77
Temkin	A_T, L mg^{-1}	6366.95	11.55
	b_T, kJ mol^{-1}	445.22	186.81
	R^2	0.87	0.95
Halsey	$q_{e\ cal}$, mg g^{-1}	79.34	101.08
	n_H	−8.59	−4.05
	K_H	32.80	14.12
	R^2	0.80	0.94
Dubinin–Radushkevich	q_m mol g^{-1}	72.25	82.30
	β, (mol $kJ^{-1})^2$	0.00005	0.00025
	R^2	0.85	0.92
Harkins–Jura	A, mg g^{-1}	3333.00	1666.67
	B	2.33	1.83
	R^2	0.61	0.74

In the Temkin model, R^2 was estimated as 0.87 for the adsorption of Cu^{2+} on to OP_b, indicating a poor-fit of the experimental data and confirming the unsuitability of this model for liquid-phase adsorption systems (Tahir et al. 2010). A relatively good-fit to the Cd^{2+} adsorption data was seen ($R^2 = 0.95$, Table 2) and the heterogeneous nature of the adsorption was further supported with a relatively high R^2 (0.94, Table 2) for Cd^{2+} adsorption using Halsey isotherm. However, a poor-fit to Cu^{2+} adsorption ($R^2 = 0.8$) was observed, as was the case in the Temkin isotherm model. The calculated equilibrium adsorption capacity was similar to the experimentally attained values ($q_{e\ exp}$ in Table 2) of 80 against 82 mg g^{-1} for Cu^{2+} and 101 against 105 for Cd^{2+}, suggesting a good presentation of equilibrium data using the Halsey isotherm model.

The D-R isotherm (Eq. (10)) differentiates between the chemical and physical adsorptions of metal ions (Dąbrowski 2001; Günay et al. 2007). The H-J isotherm model Eq. (12), on the other hand, undertakes the multilayer adsorption on adsorbents having heterogeneous pore distribution (Almeida et al. 2009; Foo and Hameed 2010).

$$\ln q_e = \ln q_m - \beta \varepsilon^2 \tag{10}$$

$$\varepsilon = RTln\,(1 + 1/C_e) \tag{11}$$

$$\frac{1}{q_e^2} = {}^{B}/_{A} - \left(\frac{1}{A}\right) \log C_e \tag{12}$$

where q_m is the maximum adsorption capacity (mg g^{-1}), β is a coefficient related to mean free energy of adsorption ($mol^2\ kJ^{-2}$), and ε is the Polanyi potential (J mol^{-1}). A linearized plot (ln q_e vs. ε) generated the values of q_m and β (Table 2). In Eq. (12), A and B are H-J constants that can be obtained from the slope and intercept values of the plot of $1/q_e^2$ vs. log C_e, given in Table 2. A relatively high value of R^2 for Cd^{2+} (0.92, Table 2), as compared to Cd^{2+} ($R^2 = 0.85$, Table 2), suggested a better fit of the D-R isotherm to its adsorption on to OP_b. The value of R^2 (0.61 and 0.74 for Cu^{2+} and Cd^{2+}, respectively) was much lower in the H-J isotherm than all other isotherm models, representing the least fit to experimental data using the H-J isotherm model.

Conclusions

Biochar derived from orange peels was used for removing Cu^{2+} and Cd^{2+} in aqueous media by performing batch experiments in triplicate. A range of batch process parameters was optimized and different isotherm models were used to model the adsorption data. Additionally, the behavior of adsorption process was analyzed by employing reaction kinetics. The OP_b showed porous and irregular surfaces, prior to sorption process, which were used to sorb metals ions onto the surfaces, as reflected by SEM images. EDX results also confirmed the successful adsorption of Cu^{2+} and Cd^{2+} on to OP_b due to strong physiochemical interactions. The abrupt changes in the FTIR spectra were observed when the OP_b was charred at 800 °C, and the number of bands representing the functional groups disappeared while new stretching bands appeared.

A rapid adsorption during the first 15–30 min followed by a slower rate of adsorption was observed for both heavy metal ions, and an equilibrium time of about half an hour was suggested for low initial metal ion concentrations (25–50 mg L^{-1}). By increasing the initial solution pH from 2.5 to 5.5, a difference in metal removal efficiency of about 22 and 35% for Cu^{2+} and Cd^{2+}, respectively, was seen with maximum metal uptake observed at the pH value of 5.0. The sorption rate and the adsorption capacity increased as the initial metal concentration increased from 25 to 200 mg L^{-1} while the optimum value for Cu^{2+} and Cd^{2+} were estimated as 82 and 105 mg g^{-1}, respectively. The removal efficiency, however, decreased from 99% against 25 mg L^{-1} to about 41 and 52% for Cu^{2+} and Cd^{2+}, respectively, against 200 mg L^{-1} of initial concentrations. The adsorption capacity decreased by increasing the OP_b dose from 0.2 to 1.4 g, while metal removal efficiency increased almost linearly with optimum OP_b dose suggested as 1.0 g for Cd^{2+}.

Among the two-parameter isotherm models used in this study, the experimental adsorption data described the best-fit for the adsorption of Cu^{2+} as follows: Langmuir > Temkin >

D-R > Halsey and Freundlich > H-J. However, for Cd^{2+}, experimental data showed the best-fit as follows: Temkin > Halsey > D-R > Langmuir > Freundlich > H-J. The adsorption data of Cu^{2+} and Cd^{2+} showed best-fit to the pseudo-second-order kinetic model with R^2 values close to unity (1.0), suggesting chemisorption nature of OP_b for adsorption. On the other hand, a relatively weak correlation to the pseudo-first-order model, with R^2 as low as 0.83 and 0.92 Cu^{2+} and Cd^{2+}, respectively, was observed. The results of the isotherm and kinetic models demonstrated the effectiveness of OP_b adsorbent for removal of Cu^{2+} and Cd^{2+} through homogeneous and heterogeneous biosorption patches on the surface of OP_b.

Acknowledgments The authors thank the Deanship of Scientific Research and RSSU at King Saud University for their technical support.

Funding information The project was financially supported by King Saud University, Vice Deanship of Research Chairs.

Compliance with ethical standards

Conflict of interest The authors declare that they have no conflict of interest.

References

Ahmad M, Rajapaksha AU, Lim JE, Zhang M, Bolan N, Mohan D, Vithanage M, Lee SS, Ok YS (2014) Biochar as a sorbent for contaminant management in soil and water: a review. Chemosphere 99: 19–33. https://doi.org/10.1016/j.chemosphere.2013.10.071

Ahmad M, Ahmad M, Usman ARA, al-Faraj AS, Abduljabbar AS, al-Wabel MI (2017) Biochar composites with nano zerovalent iron and eggshell powder for nitrate removal from aqueous solution with coexisting chloride ions. Environ Sci Pollut Res Int 25:25757–25771. https://doi.org/10.1007/s11356-017-0125-9

Ahmad M, Usman ARA, Al-Faraj AS et al (2018) Phosphorus-loaded biochar changes soil heavy metals availability and uptake potential of maize (Zea mays L.) plants. Chemosphere 194:327–339. https://doi.org/10.1016/j.chemosphere.2017.11.156

Akar E, Altinişik A, Seki Y (2013) Using of activated carbon produced from spent tea leaves for the removal of malachite green from aqueous solution. Ecol Eng 52:19–27. https://doi.org/10.1016/j.ecoleng.2012.12.032

Al-Ghouti MA, Khraisheh MAM, Allen SJ, Ahmad MN (2003) The removal of dyes from textile wastewater: a study of the physical characteristics and adsorption mechanisms of diatomaceous earth. J Environ Manag 69:229–238. https://doi.org/10.1016/j.jenvman.2003.09.005

Al-Ghouti MA, Li J, Salamh Y et al (2010) Adsorption mechanisms of removing heavy metals and dyes from aqueous solution using date pits solid adsorbent. J Hazard Mater 176:510–520. https://doi.org/10.1016/j.jhazmat.2009.11.059

Al-Homaidan AA, Al-Houri HJ, Al-Hazzani AA et al (2014) Biosorption of copper ions from aqueous solutions by Spirulina platensis biomass. Arab J Chem 7:57–62. https://doi.org/10.1016/j.arabjc.2013.05.022

Alkhashman O (2005) Study of chemical composition in wet atmospheric precipitation in Eshidiya area, Jordan. Atmos Environ 39:6175–6183. https://doi.org/10.1016/j.atmosenv.2005.06.056

Almeida CAP, Debacher NA, Downs AJ, Cottet L, Mello CAD (2009) Removal of methylene blue from colored effluents by adsorption on montmorillonite clay. J Colloid Interface Sci 332:46–53. https://doi.org/10.1016/j.jcis.2008.12.012

Amin MT, Alazba AA, Shafiq M (2017a) Removal of copper and lead using banana biochar in batch adsorption systems: isotherms and kinetic studies. Arab J Sci Eng 43:1–12. https://doi.org/10.1007/s13369-017-2934-z

Amin MT, Alazba AA, Shafiq M (2017b) Effective adsorption of methylene blue dye using activated carbon developed from the rosemary plant: isotherms and kinetic studies. Desalin Water Treat 74:336–345

Areco MM, Afonso M d S (2010) Copper, zinc, cadmium and lead biosorption by Gymnogongrus torulosus. Thermodynamics and kinetics studies. Colloids Surf B Biointerfaces 81:620–628. https://doi.org/10.1016/j.colsurfb.2010.08.014

Barakat MA (2011) New trends in removing heavy metals from industrial wastewater. Arab J Chem 4:361–377. https://doi.org/10.1016/j.arabjc.2010.07.019

Bhaumik M, Setshedi K, Maity A, Onyango MS (2013) Chromium(VI) removal from water using fixed bed column of polypyrrole/Fe_3O_4 nanocomposite. Sep Purif Technol 110:11–19. https://doi.org/10.1016/j.seppur.2013.02.037

Bilal M, Shah JA, Ashfaq T, Gardazi SMH, Tahir AA, Pervez A, Haroon H, Mahmood Q (2013) Waste biomass adsorbents for copper removal from industrial wastewater—a review. J Hazard Mater 263:322–333. https://doi.org/10.1016/j.jhazmat.2013.07.071

Budai A, Wang L, Gronli M, Strand LT, Antal MJ Jr, Abiven S, Dieguez-Alonso A, Anca-Couce A, Rasse DP (2014) Surface properties and chemical composition of corncob and Miscanthus biochars: effects of production temperature and method. J Agric Food Chem 62: 3791–3799. https://doi.org/10.1021/jf501139f

Cao X, Ma L, Gao B, Harris W (2009) Dairy-manure derived biochar effectively sorbs lead and atrazine. Environ Sci Technol 43:3285–3291. https://doi.org/10.1021/es803092k

Chen B, Chen Z (2009) Sorption of naphthalene and 1-naphthol by biochars of orange peels with different pyrolytic temperatures. Chemosphere 76:127–133. https://doi.org/10.1016/j.chemosphere.2009.02.004

Chen JP, Lin M (2001) Equilibrium and kinetics of metal ion adsorption onto a commercial H-type granular activated carbon: experimental and modeling studies. Water Res 35:2385–2394. https://doi.org/10.1016/S0043-1354(00)00521-2

Chi T, Zuo J, Liu F (2017) Performance and mechanism for cadmium and lead adsorption from water and soil by corn straw biochar. Front Environ Sci Eng 11:15. https://doi.org/10.1007/s11783-017-0921-y

Claoston N, Samsuri AW, Ahmad Husni MH, Mohd Amran MS (2014) Effects of pyrolysis temperature on the physicochemical properties of empty fruit bunch and rice husk biochars. Waste Manag Res J Int Solid Wastes Public Clean Assoc ISWA 32:331–339. https://doi.org/10.1177/0734242X14525822

Crini G, Peindy HN, Gimbert F, Robert C (2007) Removal of C.I. Basic Green 4 (Malachite Green) from aqueous solutions by adsorption using cyclodextrin-based adsorbent: kinetic and equilibrium studies. Sep Purif Technol 53:97–110. https://doi.org/10.1016/j.seppur.2006.06.018

Dąbrowski A (2001) Adsorption — from theory to practice. Adv Colloid Interf Sci 93:135–224. https://doi.org/10.1016/S0001-8686(00)00082-8

Danilchenko SN, Kalinkevich OV, Pogorelov MV et al (2011) Characterization and in vivo evaluation of chitosan-hydroxyapatite bone scaffolds made by one step coprecipitation method. J Biomed Mater Res A 96:639–647

Das SK, Guha AK (2007) Biosorption of chromium by Termitomyces clypeatus. Colloids Surf B Biointerfaces 60:46–54. https://doi.org/10.1016/j.colsurfb.2007.05.021

Dermentzis K, Christoforidis A, Valsamidou E (2011) Removal of nickel, copper, zinc and chromium from synthetic and industrial wastewater by electrocoagulation - semantic scholar. Int J Environ Sci 1:697–710

Ebrahimi R, Maleki A, Shahmoradi B, Daraei H, Mahvi AH, Barati AH, Eslami A (2013) Elimination of arsenic contamination from water using chemically modified wheat straw. Desalin Water Treat 51: 2306–2316. https://doi.org/10.1080/19443994.2012.734675

Foo KY, Hameed BH (2010) Insights into the modeling of adsorption isotherm systems. Chem Eng J 156:2–10. https://doi.org/10.1016/j.cej.2009.09.013

Greluk M, Hubicki Z (2010) Kinetics, isotherm and thermodynamic studies of reactive black 5 removal by acid acrylic resins. Chem Eng J 162:919–926. https://doi.org/10.1016/j.cej.2010.06.043

Guendy HR (2010) Treatment and reuse of wastewater in the textile industry by means of coagulation and adsorption techniques. J Appl Sci Res 6:964–972

Günay A, Arslankaya E, Tosun İ (2007) Lead removal from aqueous solution by natural and pretreated clinoptilolite: adsorption equilibrium and kinetics. J Hazard Mater 146:362–371. https://doi.org/10.1016/j.jhazmat.2006.12.034

Han R, Zou W, Li H, Li Y, Shi J (2006) Copper(II) and lead(II) removal from aqueous solution in fixed-bed columns by manganese oxide coated zeolite. J Hazard Mater 137:934–942. https://doi.org/10.1016/j.jhazmat.2006.03.016

Huang X-Y, Mao X-Y, Bu H-T, Yu XY, Jiang GB, Zeng MH (2011) Chemical modification of chitosan by tetraethylenepentamine and adsorption study for anionic dye removal. Carbohydr Res 346: 1232–1240. https://doi.org/10.1016/j.carres.2011.04.012

Inyang M, Gao B, Yao Y, Xue Y, Zimmerman AR, Pullammanappallil P, Cao X (2012) Removal of heavy metals from aqueous solution by biochars derived from anaerobically digested biomass. Bioresour Technol 110:50–56. https://doi.org/10.1016/j.biortech.2012.01.072

Inyang M, Gao B, Yao Y et al (2016) A review of biochar as a low-cost adsorbent for aqueous heavy metal removal. Crit Rev Environ Sci Technol 46:406–433. https://doi.org/10.1080/10643389.2015.1096880

Jindo K, Mizumoto H, Sawada Y, Sanchez-Monedero MA, Sonoki T (2014) Physical and chemical characterization of biochars derived from different agricultural residues. Biogeosciences 11:6613–6621. https://doi.org/10.5194/bg-11-6613-2014

Jouiad M, Al-Nofeli N, Khalifa N et al (2015) Characteristics of slow pyrolysis biochars produced from Rhodes Grass and fronds of edible date palm. J Anal Appl Pyrolysis 111:183–190. https://doi.org/10.1016/j.jaap.2014.10.024

Karim A, Kumar M, Mohapatra S, Panda C, Singh A (2015) Banana peduncle biochar: characteristics and adsorption of hexavalent chromium from aqueous solution. Int Res J Pure Appl Chem 7:1–10. https://doi.org/10.9734/IRJPAC/2015/16163

Kim Y-J, Choi J-H (2010) Improvement of desalination efficiency in capacitive deionization using a carbon electrode coated with an ion-exchange polymer. Water Res 44:990–996. https://doi.org/10.1016/j.watres.2009.10.017

Kim KH, Kim J-Y, Cho T-S, Choi JW (2012) Influence of pyrolysis temperature on physicochemical properties of biochar obtained from the fast pyrolysis of pitch pine (Pinus rigida). Bioresour Technol 118:158–162. https://doi.org/10.1016/j.biortech.2012.04.094

Kiran I, Akar T, Ozcan AS, Ozcan A, Tunali S (2006) Biosorption kinetics and isotherm studies of acid red 57 by dried Cephalosporium aphidicola cells from aqueous solutions. Biochem Eng J 31:197–203. https://doi.org/10.1016/j.bej.2006.07.008

Kloss S, Zehetner F, Dellantonio A, Hamid R, Ottner F, Liedtke V, Schwanninger M, Gerzabek MH, Soja G (2012) Characterization of slow pyrolysis biochars: effects of feedstocks and pyrolysis temperature on biochar properties. J Environ Qual 41:990–1000. https://doi.org/10.2134/jeq2011.0070

Krishnani KK, Meng X, Christodoulatos C, Boddu VM (2008) Biosorption mechanism of nine different heavy metals onto biomatrix from rice husk. J Hazard Mater 153:1222–1234. https://doi.org/10.1016/j.jhazmat.2007.09.113

Kumar PR, Chaudhari S, Khilar KC, Mahajan SP (2004) Removal of arsenic from water by electrocoagulation. Chemosphere 55:1245–1252

Kumar PS, Ramakrishnan K, Gayathri R (2010) Removal of nickel (II) from aqueous solutions by Ceralite IR 120 cationic exchange resins. J Eng Sci Technol 5:232–243

Lammers K, Arbuckle-Keil G, Dighton J (2009) FT-IR study of the changes in carbohydrate chemistry of three New Jersey pine barrens leaf litters during simulated control burning. Soil Biol Biochem 41: 340–347. https://doi.org/10.1016/j.soilbio.2008.11.005

Langmuir I (1918) The adsorption of gases on plane surface of glass, mica and platinum. J Am Chem Soc 40:1361–1403. https://doi.org/10.1021/ja02242a004

Lin Y, Choi D, Wang J, Bontha J (2009) Chapter 14 - nanomaterials-enhanced electrically switched ion exchange process for water treatment. In: Savage N, Diallo M, Duncan J et al (eds) Nanotechnology applications for clean water. William Andrew Publishing, Boston, pp 179–189

Liu B-J, Ren Q-L (2006) Sorption of levulinic acid onto weakly basic anion exchangers: equilibrium and kinetic studies. J Colloid Interface Sci 294:281–287. https://doi.org/10.1016/j.jcis.2005.07.042

Ma X, Zhou B, Budai A, Jeng A, Hao X, Wei D, Zhang Y, Rasse D (2016) Study of biochar properties by scanning electron microscope – energy dispersive X-ray spectroscopy (SEM-EDX). Commun Soil Sci Plant Anal 47:593–601. https://doi.org/10.1080/00103624.2016.1146742

Malkoc E, Nuhoglu Y, Dundar M (2006) Adsorption of chromium(VI) on pomace—an olive oil industry waste: batch and column studies. J Hazard Mater 138:142–151. https://doi.org/10.1016/j.jhazmat.2006.05.051

Mary GS, Sugumaran P, Niveditha S et al (2016) Production, characterization and evaluation of biochar from pod (Pisum sativum), leaf (Brassica oleracea) and peel (Citrus sinensis) wastes. Int J Recycl Org Waste Agric 5:43–53. https://doi.org/10.1007/s40093-016-0116-8

Mavrov V, Stamenov S, Todorova E, Chmiel H, Erwe T (2006) New hybrid electrocoagulation membrane process for removing selenium from industrial wastewater. Desalination 201:290–296. https://doi.org/10.1016/j.desal.2006.06.005

Mohsen MS, Jaber JO, Afonso MD (2003) Desalination of brackish water by nanofiltration and reverse osmosis. Desalination 157:167. https://doi.org/10.1016/S0011-9164(03)00397-7

O'Connell DW, Birkinshaw C, O'Dwyer TF (2008) Heavy metal adsorbents prepared from the modification of cellulose: a review. Bioresour Technol 99:6709–6724. https://doi.org/10.1016/j.biortech.2008.01.036

Ofomaja AE, Ho Y-S (2007) Equilibrium sorption of anionic dye from aqueous solution by palm kernel fibre as sorbent. Dyes Pigments 74: 60–66. https://doi.org/10.1016/j.dyepig.2006.01.014

Özacar M, Şengil İA (2003) Adsorption of reactive dyes on calcined alunite from aqueous solutions. J Hazard Mater 98:211–224. https://doi.org/10.1016/S0304-3894(02)00358-8

Purkayastha D, Mishra U, Biswas S (2014) A comprehensive review on Cd(II) removal from aqueous solution. J Water Process Eng 2:105–128. https://doi.org/10.1016/j.jwpe.2014.05.009

Putra WP, Kamari A, Yusoff SNM et al (2014) Biosorption of Cu(II), Pb(II) and Zn(II) ions from aqueous solutions using selected waste materials: adsorption and characterisation studies. J Encapsulation Adsorpt Sci 04:25–35. https://doi.org/10.4236/jeas.2014.41004

Rafiq S, Kaul R, Sofi SA, Bashir N, Nazir F, Ahmad Nayik G (2016) Citrus peel as a source of functional ingredient: a review. J Saudi Soc Agric Sci 17:351–358. https://doi.org/10.1016/j.jssas.2016.07.006

Rathinam A, Maharshi B, Janardhanan SK, Jonnalagadda RR, Nair BU (2010) Biosorption of cadmium metal ion from simulated wastewaters using Hypnea valentiae biomass: a kinetic and thermodynamic study. Bioresour Technol 101:1466–1470. https://doi.org/10.1016/j.biortech.2009.08.008

Shafiq M, Alazba AA, Amin MT (2018) Removal of heavy metals from wastewater using date palm as a biosorbent: a comparative review. Sains Malays 47:35–49. https://doi.org/10.17576/jsm-2018-4701-05

Snoeyink VL, Jenkins D (1980) Water chemistry. JohnWiley & Sons, New York

Srivastava VC, Mall ID, Mishra IM (2008) Removal of cadmium(II) and zinc(II) metal ions from binary aqueous solution by rice husk ash. Colloids Surf Physicochem Eng Asp 312:172–184. https://doi.org/10.1016/j.colsurfa.2007.06.048

Suliman W, Harsh JB, Abu-Lail NI, Fortuna AM, Dallmeyer I, Garcia-Perez M (2016) Influence of feedstock source and pyrolysis temperature on biochar bulk and surface properties. Biomass Bioenergy 84:37–48. https://doi.org/10.1016/j.biombioe.2015.11.010

Tag AT, Duman G, Ucar S, Yanik J (2016) Effects of feedstock type and pyrolysis temperature on potential applications of biochar. J Anal Appl Pyrolysis 120:200–206. https://doi.org/10.1016/j.jaap.2016.05.006

Tahir H, Hammed U, Sultan M, Jahanzeb Q (2010) Batch adsorption technique for the removal of malachite green and fast green dyes by using montmorillonite clay as adsorbent. Afr J Biotechnol 9:8206–8214. https://doi.org/10.5897/AJB10.911

Tan G, Xiao D (2009) Adsorption of cadmium ion from aqueous solution by ground wheat stems. J Hazard Mater 164:1359–1363. https://doi.org/10.1016/j.jhazmat.2008.09.082

Temkin MJ, Pyzhev V (1940) Kinetics of ammonia synthesis on promoted iron catalysts. Acta Physicochim URSS 12:217–222

Tong X, Li J, Yuan J, Xu R (2011) Adsorption of Cu(II) by biochars generated from three crop straws. Chem Eng J 172:828–834. https://doi.org/10.1016/j.cej.2011.06.069

Tunali S, Özcan AS, Özcan A, Gedikbey T (2006) Kinetics and equilibrium studies for the adsorption of Acid Red 57 from aqueous solutions onto calcined-alunite. J Hazard Mater 135:141–148. https://doi.org/10.1016/j.jhazmat.2005.11.033

Usman ARA, Ahmad M, El-Mahrouky M et al (2016) Chemically modified biochar produced from conocarpus waste increases NO3 removal from aqueous solutions. Environ Geochem Health 38:511–521. https://doi.org/10.1007/s10653-015-9736-6

Uzunoğlu D, Gürel N, Özkaya N, Özer A (2014) The single batch biosorption of copper(II) ions on Sargassum acinarum. Desalin Water Treat 52:1514–1523. https://doi.org/10.1080/19443994.2013.789403

Volesky B, Holan ZR (1995) Biosorption of heavy metals. Biotechnol Prog 11:235–250. https://doi.org/10.1021/bp00033a001

Xu X, Cao X, Zhao L (2013) Comparison of rice husk- and dairy manure-derived biochars for simultaneously removing heavy metals from aqueous solutions: role of mineral components in biochars. Chemosphere 92:955–961. https://doi.org/10.1016/j.chemosphere.2013.03.009

Yavuz M, Gode F, Pehlivan E et al (2008) An economic removal of Cu^{2+} and Cr^{3+} on the new adsorbents: pumice and polyacrylonitrile/pumice composite. Chem Eng J 137:453–461. https://doi.org/10.1016/j.cej.2007.04.030

Yuan J-H, Xu R-K, Zhang H (2011) The forms of alkalis in the biochar produced from crop residues at different temperatures. Bioresour Technol 102:3488–3497. https://doi.org/10.1016/j.biortech.2010.11.018